Electron leakage and its suppression via deep-well structures in 4.5- to 5.0-μm-emitting quantum cascade lasers

Dan Botez
Jae Cheol Shin
University of Wisconsin–Madison
Department of Electrical and Computer Engineering
Madison, Wisconsin 53706
E-mail: botez@engr.wisc.edu

Sushil Kumar
Lehigh University
Department of Electrical and Computer Engineering
Bethlehem, Pennsylvania 18015

Luke J. Mawst
University of Wisconsin–Madison
Department of Electrical and Computer Engineering
Madison, Wisconsin 53706

Igor Vurgaftman
Jerry R. Meyer, MEMBER SPIE
Naval Research Laboratory
Code 5613
Washington, DC 20375

Abstract. The equations for threshold-current density J_{th} and external differential quantum efficiency η_d of quantum cascade lasers (QCLs) are modified to include electron leakage and the electron-backfilling term corrected to take into account *hot* electrons in the injector. We show that by introducing both deep quantum wells and tall barriers in the active regions of 4.8-μm-emitting QCLs, and by tapering the conduction-band edge of both injector and extractor regions, one can significantly reduce electron leakage. The characteristic temperatures for J_{th} and η_d, denoted by T_0 and T_1, respectively, are found to reach values as high as 278 and 285 K over the 20 to 90°C temperature range, which means that J_{th} and η_d display $\approx$ 2.3 slower variation than conventional 4.5- to 5.0-μm-emitting, high-performance QCLs over the same temperature range. A model for the thermal excitation of hot injected electrons from the upper laser level to the upper active-region energy states, wherefrom some relax to the lower active-region states and some are scattered to the upper miniband, is used to estimate the leakage current. Estimated T_0 values are in good agreement with experiment for both conventional QCLs and deep-well QCLs. The T_1 values are justified by increases in both electron leakage and waveguide loss with temperature. [DOI: 10.1117/1.3509368]

Subject terms: quantum cascade lasers; mid infrared; threshold-current characteristic temperature; slope-efficiency characteristic temperature; electron leakage current; hot electrons.

Paper 100339SSR received Apr. 19, 2010; revised manuscript received Sep. 21, 2010; accepted for publication Sep. 24, 2010; published online Dec. 1, 2010.

1 Introduction

The device core of a conventional quantum cascade laser[1] (QCL) is composed of a superlattice of quantum wells (QWs) and barriers of fixed alloy compositions. As a consequence, state-of-the-art devices optimized for high continuous-wave (cw) power and emitting in the 4.5- to 5.0-μm range[2,3] suffer from substantial thermally activated electron leakage from the upper laser level to the continuum. This leakage is evidenced by high sensitivity of their electro-optical characteristics to heatsink temperature variations at and above room temperature (RT) (i.e., above 300 K). That is, the characteristic temperature coefficient T_0 for the threshold-current density J_{th} [defined by $J_{th}(T_{ref} + \Delta T) = J_{th}(T_{ref}) \exp(\Delta T/T_0)$, where $T_{ref} + \Delta T$ is the heatsink temperature and T_{ref} is the reference heatsink temperature (e.g., 300 K)] is found to have low values of $\approx$140 K for 4.6-μm-emitting devices.[2,3] Similarly, the characteristic temperature coefficient T_1 for the differential quantum efficiency η_d, defined by $\eta_d(T_{ref} + \Delta T) = \eta_d(T_{ref}) \exp(-\Delta T/T_1)$, is also found to have a low value $\approx$140 K for 4.6-μm-emitting devices.[2] These low values for both T_0 and T_1 are indirectly attributable to the small energy differential, $\delta E = 150$ to 250 meV, between the upper laser level and the top of the exit barrier.[3,4] In turn, the maximum wallplug efficiency $\eta_{wp,max}$ in cw operation at RT, for light emitted from the front facet of devices with high-reflectivity-coated back facets, has typical values[5,6] of $\approx$12%, far short of theoretically predicted limits[7] of $\approx$28% at $\lambda \approx 4.6$ μm. In contrast, at cryogenic temperatures (40 to 80 K), where thermally activated electron leakage is negligible, maximum pulsed wallplug efficiency values as high as 50% have been achieved,[8,9] in close agreement with the theoretically predicted upper limit[10] of $\approx$60% at $\lambda \approx 4.6$ μm and 80-K heatsink temperature.

By taking advantage of the flexibility of the metal-organic chemical vapor deposition (MOCVD) method to easily grow epitaxial QWs and barrier layers of multiple compositions in the QCL core region, we have implemented the deep-well (DW) concept[11] in InP-based devices[12,13] and thus obtained δE values as high as 450 meV.[12] In turn, electron leakage in and out of the active regions is substantially suppressed, which results in QCLs whose electro-optical characteristics are much less sensitive to temperature[12,13] than those for conventional devices.

After deriving equations for J_{th} and η_d that take into account both leakage and backfilling currents, we discuss the DW concept, key results from DW QCLs, and the effects of tapering the conduction-band edge for the extractor and injection regions on the DW QCL's performance. We then show that by using the modified J_{th} and η_d equations, in conjunction with a model for electron thermal excitation in and out of the active region, one can obtain good

0091-3286/2010/$25.00 © 2010 SPIE

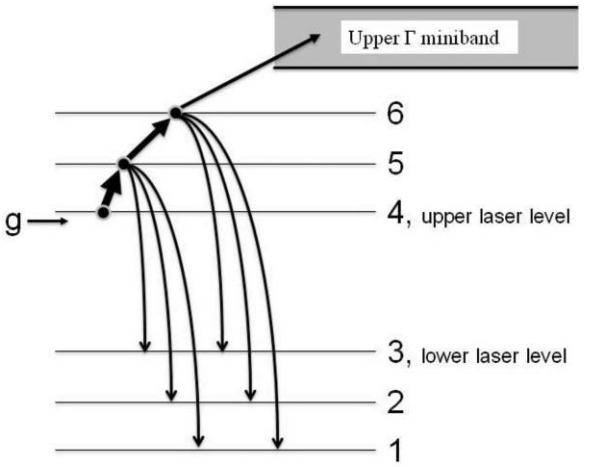

Fig. 1 Schematic representation of the primary leakage paths for electrons injected into the upper laser level of a 4.5- to 5.5-μm-emitting QCL of the DPR design. Here *g* is the injector-region ground state, 1 through 6 are energy states in the active region, and the area marked as upper Γ miniband corresponds to the energy states in the upper Γ miniband of the extractor region.

agreement between calculated and experimental values for T_0 in both conventional and DW-type QCLs. For optimized DW QCLs, front-facet, 300-K cw $\eta_{wp,max}$ values >20% are projected.

2 Modified Equations for the Threshold Current and the Differential Quantum Efficiency

Figure 1 schematically shows the primary leakage paths in and out of the active region of a QCL of the double-phonon-resonance (DPR) design. Following the injection of electrons into the upper laser level (i.e., state 4), some are thermally excited to the active region's (AR's) next-higher energy level (state 5), wherefrom they either relax to the lower-energy AR states (i.e., states 3, 2, and 1) or are further excited to the next-higher level (i.e., state 6). For state 6, electron leakage consists of both relaxation to the states 3, 2, and 1 and excitation to the upper-Γ-miniband states and subsequently to the continuum. While other parallel leakage paths exist, their currents should be negligible. On the one hand, at threshold the tunneling-injection efficiencies are close to unity, and the QW/barrier structures (e.g., $In_{0.67}Ga_{0.33}As/Al_{0.64}In_{0.36}As$) of conventional, high-performance 4.5- to 5.0-μm-emitting devices substantially prevent electron injection into the upper AR levels.[4] On the other hand, thermal excitation from state 4 to state 6 and from state 5 to the upper-Γ-miniband states *and* relaxation from state 6 to the lower-Γ-miniband states are negligible because of relatively large energy differences and/or poor wave-function overlap.

The conventional equations[1] for the threshold and differential quantum efficiency should be modified to include the effects of electron leakage and, since the electrons in the injector are found to be hot,[14] for electron backfilling as well. We assume that the efficiency of tunneling injection from the injector to the upper laser level[1] (η_{inj}) is unity. The threshold-current density is then the sum of J_{th} in the absence of backfilling and electron leakage ($J_{0,th}$) and the current densities required *at threshold* to compensate for backfilling ($J_{bf,th}$) and electron leakage ($J_{leak,th}$), each of which is defined below:

$$J_{0,th} = \frac{q}{\tau_{up}} \frac{\alpha_{tot}}{g_c N_p}, \tag{1}$$

$$J_{bf,th} = \frac{q}{\tau_{up}} \left[n_s \exp\left(-\frac{\Delta_{inj} + \hbar\omega_{LO}[(T_{eg}/T) - 1]}{kT_{eg}} \right) + \left(\frac{n_5}{\tau_{53}} + \frac{n_6}{\tau_{63}} \right) \tau_3 \right], \tag{2}$$

$$J_{leak,th} = \frac{q}{\tau_{5,leak}} n_5 + \frac{q}{\tau_{6,leak}} n_6, \tag{3}$$

where $\tau_{up} = \tau_4(1 - \tau_3/\tau_{43})$ is the *effective* upper-state lifetime[7] due to both inelastic and elastic scattering, α_{tot} is the sum of the mirror (α_m) and waveguide (α_w) losses, g_c is the modal gain cross section per period,[7] N_p is the number of periods, n_s is the electron sheet density in the injector, Δ_{inj} is the energy difference between the lower laser level and the ground state in the injector of the subsequent stage in the QCL structure, $\hbar\omega_{LO}$ is the longitudinal-optical (LO) phonon energy, T_{eg} is the electronic temperature in the injector,[14] $n_{LO} = 1/[\exp(\hbar\omega_{LO}/kT) - 1]$ is the occupation number of phonons (assumed to be in thermal equilibrium with the lattice at temperature *T*), τ_{53} (τ_{63}) is the lifetime corresponding to electron relaxation from state 5 (6) to state 3, τ_3 is the lifetime in the lower laser level, and n_5 (n_6) and $\tau_{5,leak}$ ($\tau_{6,leak}$) are the sheet densities and electron-leakage lifetimes, respectively, corresponding to the AR's upper states 5 and 6. More specifically, $\tau_{5,leak} = (1/\tau_{53} + 1/\tau_{52} + 1/\tau_{51})^{-1}$ and $\tau_{6,leak} = (1/\tau_{6,um} + 1/\tau_{63} + 1/\tau_{62} + 1/\tau_{61})^{-1}$, where $\tau_{6,um}$ is the lifetime corresponding to thermal excitation from state 6 to all the states in the upper Γ miniband [see Eq. (16), Sec. 5], and the other lifetimes correspond to relaxation from states 5 and 6 to states 3, 2, and 1. Here n_5 and n_6 are as defined in the section dedicated to estimating T_0 and T_1 values (Sec. 5). By definition, $J_{0,th} + J_{bf,th} = qn_{4,th}/\tau_4$, where $n_{4,th}$ is the sheet density in the upper laser level at threshold, and $\tau_4 = (1/\tau_{43} + 1/\tau_{42} + 1/\tau_{41})^{-1}$ is the lifetime in that level, reflecting electron relaxation to states 3, 2, and 1. We determine the backfilling-current term by starting with the total current flow across the QCL structure, written as

$$J \equiv J_0 + J_{bf} + J_{leak},$$

where

$$J_0 + J_{bf} \equiv \frac{q}{\tau_4} n_4 \tag{4}$$

is the "useful" current flowing through the upper laser level (state 4), and

$$J_{leak} \equiv \frac{q}{\tau_{5,leak}} n_5 + \frac{q}{\tau_{6,leak}} n_6 \tag{5}$$

constitutes the leakage current in general (i.e., not just at threshold).

A steady-state rate equation for the lower laser level (state 3) can be written as

$$\frac{n_3}{\tau_3} = \left(\frac{n_5}{\tau_{53}} + \frac{n_6}{\tau_{63}} + \frac{n_4}{\tau_{43}} \right) + \left(\frac{n_2}{\tau_{23}} + \frac{n_1}{\tau_{13}} \right), \tag{6}$$

where n_3, n_2, and n_1 are the sheet densities in the AR's lower states 3, 2, and 1; and τ_{23} (τ_{13}) is the lifetime corresponding to thermal excitation from state 2 (1) to state 3 [Eq. (16), Sec. 5].

Substituting Eq. (4) into Eq. (6), we get

$$\Delta n_{43} \equiv n_4 - n_3 = \frac{J_0 + J_{\rm bf}}{q}\tau_4\left(1 - \frac{\tau_3}{\tau_{43}}\right) - \left(\frac{n_2}{\tau_{23}} + \frac{n_1}{\tau_{13}}\right)\tau_3 - \left(\frac{n_5}{\tau_{53}} + \frac{n_6}{\tau_{63}}\right)\tau_3,$$

which, by using the $\tau_{\rm up}$ definition, can be rewritten as

$$J_0 + J_{\rm bf} = \frac{q}{\tau_{\rm up}}\left[\Delta n_{43} + \left(\frac{n_2}{\tau_{23}} + \frac{n_1}{\tau_{13}}\right)\tau_3 + \left(\frac{n_5}{\tau_{53}} + \frac{n_6}{\tau_{63}}\right)\tau_3\right]. \quad (7)$$

From Eq. (7), we can separate the terms as

$$J_0 = \frac{q}{\tau_{\rm up}}\Delta n_{43}, \quad (8)$$

which is the current needed in the absence of backfilling, and

$$J_{\rm bf} = \frac{q}{\tau_{\rm up}}\left[\left(\frac{n_2}{\tau_{23}} + \frac{n_1}{\tau_{13}}\right)\tau_3 + \left(\frac{n_5}{\tau_{53}} + \frac{n_6}{\tau_{63}}\right)\tau_3\right], \quad (9)$$

which is the extra current required due to backfilling of the lower laser level (state 3).

The backfilling expression in Eq. (9) can be further simplified if we make the following assumptions: (a) states 1 and 2 are strongly coupled to the injector miniband, so that the miniband states and states 1 and 2 are in thermal equilibrium, all sharing a common electronic temperature $T_{\rm eg}$,[14] and (b) the backfilling of the lower laser level from states 1 and 2 occurs primarily via LO-phonon absorption, just like the thermal excitation from the upper laser level to the upper AR states [Eq. (16), Sec. 5]. Then we can write

$$n_2 \approx n_s \exp\left(-\frac{\Delta_{\rm inj} - E_{32}}{kT_{\rm eg}}\right),$$

$$n_1 \approx n_s \exp\left(-\frac{\Delta_{\rm inj} - E_{31}}{kT_{\rm eg}}\right),$$

$$\tau_{23} \approx \tau_{32} \exp\left(\frac{E_{32} - \hbar\omega_{\rm LO}}{kT_{\rm eg}}\right)\left(\frac{1 + n_{\rm LO}}{n_{\rm LO}}\right),$$

$$\tau_{13} \approx \tau_{31} \exp\left(\frac{E_{31} - \hbar\omega_{\rm LO}}{kT_{\rm eg}}\right)\left(\frac{1 + n_{\rm LO}}{n_{\rm LO}}\right), \quad (10)$$

where E_{31} (E_{32}) is the energy difference between state 3 and state 1 (2), and it is larger than the LO-phonon energy, $\hbar\omega_{\rm LO}$. Substituting Eq. (10) into Eq. (9) and noting that $\tau_3 = \tau_{32}\tau_{31}/(\tau_{32} + \tau_{31})$, we get the final expression for the backfilling current at threshold [i.e., Eq. (2)].

For the external differential quantum efficiency $\eta_{\rm d}$, by using the rate equations for a four-level system that includes electron leakage, and by defining a *differential* pumping efficiency at threshold, $\eta_{\rm p} = (J_{0,\rm th} + J_{\rm bf,th})/(J_{0,\rm th} + J_{\rm bf,th} + J_{\rm leak,th})$, we obtain

$$\eta_{\rm d} = \eta_{\rm p}\eta_{\rm tr}\frac{\alpha_{\rm m}}{\alpha_{\rm m} + \alpha_{\rm w}}N_p = \eta_{\rm i}\frac{\alpha_{\rm m}}{\alpha_{\rm m} + \alpha_{\rm w}}N_p, \quad (11)$$

where $\eta_{\rm tr}$ is the differential efficiency of the lasing transition,[7] and $\eta_{\rm i}$, the product of $\eta_{\rm p}$ and $\eta_{\rm tr}$, is the *differential* internal efficiency per period. Here $\eta_{\rm i}$ should not confused either with the tunneling-injection efficiency[1] $\eta_{\rm inj}$, assumed here to be unity, or with the (overall) internal quantum efficiency. Just as in the case of interband-transition devices,[15] the factor multiplying the ratio of mirror losses to total losses in the $\eta_{\rm d}$ expression is a differential quantity.

Since $\eta_{\rm tr}$ is virtually temperature-independent, the temperature dependence of $\eta_{\rm d}$ is dictated by the temperature variation of both $\eta_{\rm p}$ and α_w. These account for the experimentally observed drop in $\eta_{\rm d}$ with increasing temperature, especially above 300 K (i.e., the parameter T_1). We also note that for a given heatsink temperature, changing the mirror loss $\alpha_{\rm m}$ by varying the cavity length L or front-facet reflectivity $R_{\rm f}$ will alter the differential internal efficiency value, since the quantity $J_{0,\rm th}$ in the expression for $\eta_{\rm p}$ includes $\alpha_{\rm m}$. The fact that $\eta_{\rm i}$ depends on L and $R_{\rm f}$ implies, in turn, that a conventional cavity-length[16] or reflectivity[17] study to derive $\eta_{\rm i}$ and $\alpha_{\rm w}$ from plots of $1/\eta_{\rm d}$ versus L or $1/\eta_{\rm d}$ versus $1/\alpha_{\rm m}$, with L or $R_{\rm f}$ varied over wide ranges, is likely to provide incorrect results for both $\eta_{\rm i}$ and $\alpha_{\rm w}$. Furthermore, since α_w clearly appears to increase with temperature, as deduced in Sec. 5, it may also increase with increasing α_m. That is, at and above room temperature the correct value for $\alpha_{\rm w}$ has to be determined by a different method than those conventional used, which are useful only at cryogenic temperatures.

3 The Deep-Well Concept

We initially grew a strain-compensated InP-based, 5.4-μm QCL structure of published design,[18] from which we obtained[19] RT lasing results comparable to the best results reported from 5.3-μm devices of same injector-doping level (2×10^{17} cm^{-3}). Since the optimal growth temperature range for MOCVD (630 to 660°C) is much higher than for either gas-source molecular beam epitaxy (MBE) or MBE (500 to 530°C), it has been difficult to use MOCVD to grow the highly strained structures required for lasing below 5 μm. Therefore we designed a structure, based on deep QWs in the active region, to lase at ≈4.7 μm though grown at the same temperature (630°C) used to obtain RT lasing at 5.4 μm. Basically, only the QWs in the active region are deep, as required for 4.7-μm emission (Fig. 2). Then, for strain compensation, the Al content in the barriers in and around the AR is increased from 56% to 75%, which provides much taller barriers than in conventional 4.6- to 4.8-μm QCLs.[2–6]

Another modification from conventional QCL structures is that the extractor region (i.e., the region just beyond the exit barrier) has a tapered conduction-band edge (CBE)[12] that

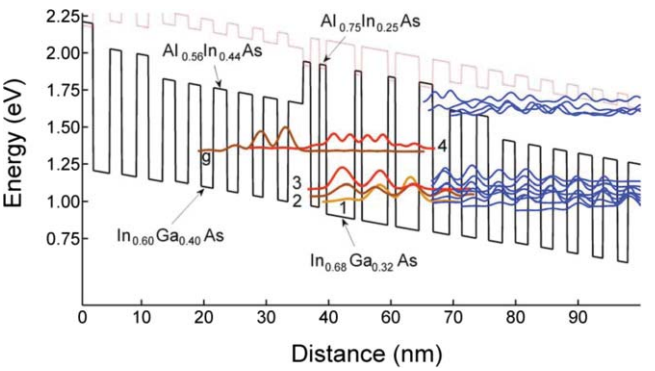

Fig. 2 Conduction-band diagram and relevant wave functions for a deep-well 4.7-μm QCL.[12]

further helps to suppress electron leakage. This occurs because the wave functions corresponding to low-energy states in the upper miniband are pushed away from the AR, so that they have negligible overlap with the wave function for the upper energy state 6. The tapered-CBE extractor region is composed of an $In_{0.66}Ga_{0.34}As$ well, an $Al_{0.65}In_{0.35}As$ barrier, an $In_{0.64}Ga_{0.36}As$ well, and an $Al_{0.65}In_{0.35}As$ barrier. We further suppress electron leakage by also tapering the CBE of the injector region.[13] The effects of tapering the CBE (in both the extractor and the injector regions) on electron leakage are made clear in the next section.

Advantages of the DW-type 4.8-μm QCL over conventional 4.6- to 4.8-μm structures[2,3] include: (1) much greater design flexibility, since highly strained layers are limited to the active region; (2) much less carrier leakage from the active QWs, since the barrier layers in and around the AR are taller (e.g., the δE value is 200 to 300 meV larger than in conventional devices). That in turn leads to much higher T_0 and T_1, and potentially superior cw performance. Furthermore, ARs that suppress electron leakage are quite relevant to the development of highly efficient intersubband quantum box (IQB) lasers,[20] since a longer upper-laser-level lifetime will make the devices much more sensitive to electron leakage. Thus, DW-QCL development is being pursued not only to improve the device performance and reliability, but also as a means for fulfilling the promise of IQB devices for achieving cw wallplug efficiencies as high as 50% at room temperature.[21]

4 Device Structures and Results

Figure 3 compares the band diagrams and relevant wave functions of a conventional QCL[3] with those for an optimized DW QCL,[13] both being of the DPR design for depopulation of the lower laser level. We see first that increasing the barrier heights increases the energy difference E_{54} between the upper laser level (state 4) and the next-highest AR energy level (state 5), from 46 meV to 60 meV. It is shown below that this significantly reduces the carrier leakage associated with thermal excitation to state 5, followed by relaxation to the lower AR states 3, 2, and 1. For high-performance QCLs with the lower lasing level depopulated via the nonresonant extraction (NRE) design,[2] E_{54} values as high as 63 meV have been reported.[6] However, the energy difference E_{65} between states 5 and 6 is only about 40 meV in such devices,[4] as compared to $\geq$80 meV for the DPR-design QCLs in Fig. 3. A lower E_{65} in turn leads to easy carrier escape to the continuum, as attested by the observation of relatively small values for both T_0 and T_1 ($\approx$140 K).[2]

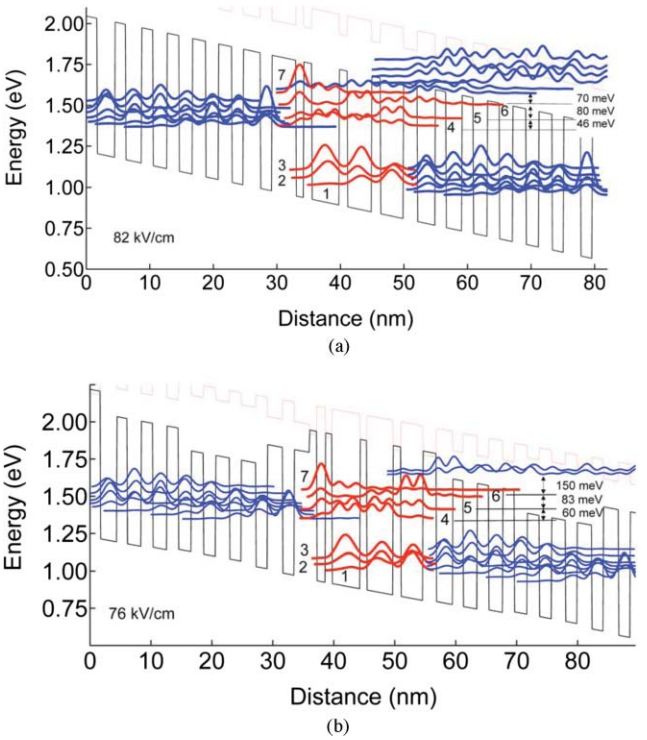

Fig. 3 Conduction-band profile and key wave functions for: (a) conventional QCL[3] emitting at 4.6 μm, (b) deep-well QCL[13] emitting at $\lambda = 4.8$ μm. The upper laser level is labeled 4, while 5, 6, and 7 are higher energy states in the active region. The band profile at the top of each figure corresponds to the X valley.

A second major difference is that the energy separation between state 6 and the bottom state of the upper Γ miniband in the extractor region, $E_{um,6}$, increases from 70 meV to 150 meV. This large enhancement occurs mostly because tapering the injector region causes the lowest state of the upper miniband to be drawn away from the extractor region, as seen in Fig. 4(c). As a consequence, electron leakage to the continuum, via thermal excitation from state 6 to the states of the upper Γ miniband, is completely suppressed.

We also note that while for conventional QCLs state 7 is strongly coupled to states in the upper miniband and thus becomes a conduit for leakage to the continuum, for DW QCLs state 7 has poor overlap with upper-miniband states and thus plays no role in electron leakage.

In order to clarify how tapering the injector- and extractor-region conduction-band edges affects electron leakage, Fig. 4 illustrates three cases: (a) DW structure with no CBE tapering, (b) DW structure with tapered CBE extractor, and (c) DW structure with tapered CBE for both the extractor and the injector. For fairness, the structures of cases (a) and (b) were designed to have the same emission wavelength ($\lambda = 4.63$ μm) and E_{54} value (60 meV) as for the published design of structure (c) in Ref. 13. Furthermore, the $J_{0,th}$ figure of merit $(z_{43})^2\tau_{up}$, where z_{43} is the dipole matrix element of the radiative transition, is found to have basically the same value in all three structures ($\approx$2.5 nm^2 ps).

In case (a) with no CBE tapering, E_{65} remains basically the same ($\approx$85 meV) as in (b) and (c), while $E_{um,6}$ has a significantly smaller value than in (c) (70 versus 150 meV), which is comparable to that for conventional DPR-design QCLs [Fig. 3(a)]. That is, the deep wells by themselves bring about a significant increase in E_{54} compared to the conventional QCL (from 46 to 60 meV), which has a primary influence on electron leakage. Tapering the extractor-region CBE causes $E_{um,6}$ to increase from 70 meV to 81 meV, besides decreasing the wave-function overlap between state 6 and the upper-miniband bottom state, um1. The latter occurs because the intermediate-height barriers introduced in the extractor region push the um1 wave function away from the AR. Both effects act to significantly reduce electron leakage via scattering from state 6 to the upper miniband. More specifically, the scattering time from state 6 to the upper miniband, $\tau_{6,um}$, as calculated using Eq. (16) in Sec. 5, increases from 9.4 ps in the case of no CBE tapering [Fig. 4(a)] to 33 ps in the case of tapered CBE in the extractor [Fig. 4(b)]. Finally, from Fig. 4(c) it is clear that tapering the injection-region CBE causes the um1 wave function to be drawn away from the

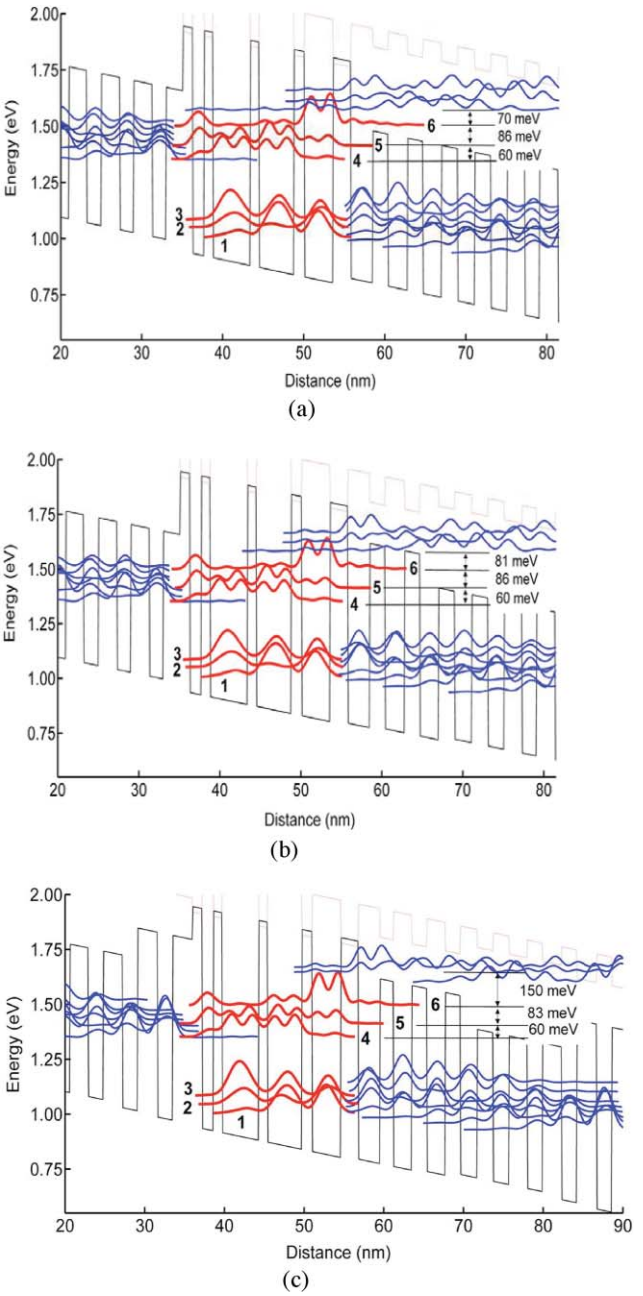

Fig. 4 Conduction-band profile and key wave functions for deep-well QCLs with: (a) no conduction band edge (CBE) tapering; (b) tapered CBE in the extractor; (c) tapered CBE in both extractor and injector.

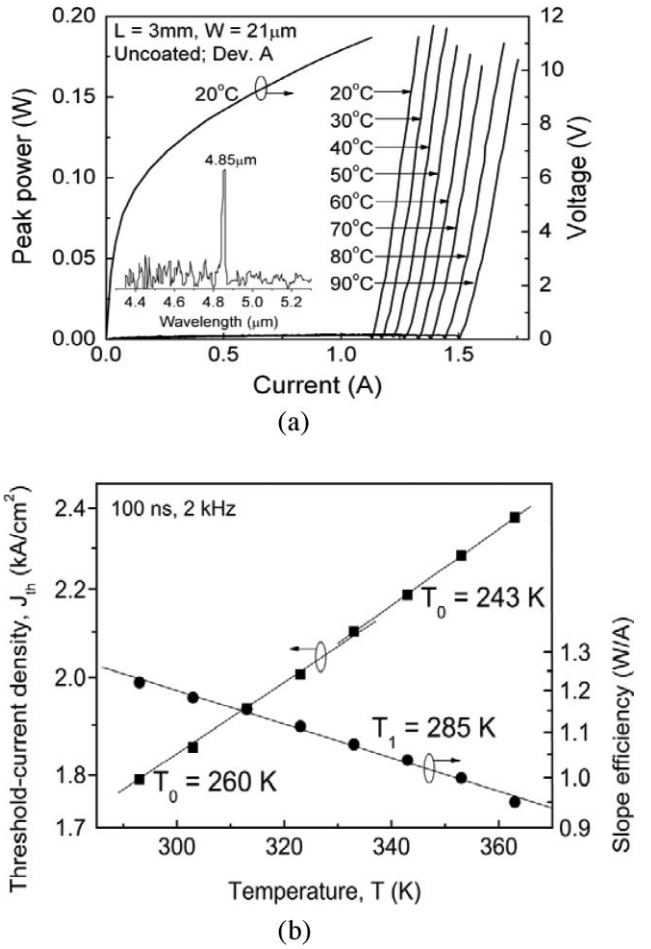

Fig. 5 Deep-well QCLs[13]: (a) Pulsed *L-I* curves as the heatsink temperature T_h varies. Inset: spectrum. (b) Plots of J_{th} and the slope efficiency η_s as functions of T_h. Here T_0 and T_1 are characteristic temperatures for J_{th} and η_s.

extractor region, which in turn dramatically increases $E_{um,6}$ (from 81 meV to 150 meV). The result is that electron leakage to the upper miniband is *de facto* shut off, as the calculated $\tau_{6,um}$ reaches values of ≈500 ps.

The electro-optical characteristics for the DW QCLs whose conduction-band diagram is displayed in Fig. 3(b) are shown in Fig. 5. The details of the laser structure are provided in Ref. 13, and details of the crystal growth are provided in Ref. 22.

Ridge-waveguide devices were mounted episide up on Cu blocks and measured in pulsed mode (100 ns, 2 kHz). The value of J_{th} at 20°C is 1.78 kA/cm^2, at a threshold voltage of 11.2 V, which is comparable to that for conventional devices. The characteristic temperature T_0 is 260 and 243 K over the 20 to 60°C and 60 to 90°C heatsink temperature ranges, respectively. Another device with somewhat higher J_{th} (1.87 kA/cm^2 at 20°C) exhibited T_0 = 278 K over the entire 20 to 90°C temperature range.[13] By comparison, T_0 for a high-performance conventional 4.6-μm QC laser[3] is only 143 K over the same temperature range. Both deep-well devices displayed a characteristic temperature for slope efficiency, T_1, of 285 K over the 20 to 90°C range [Fig. 5(b)], as compared to only ≈140 K for 4.6- to 4.8-μm QCLs operating over the 20 to 60°C (Ref. 2) and 0 to 50°C (Ref. 23) temperature ranges. While T_0 ≈ 200 K has been observed for devices with low-doped injectors [n_s = (0.5 to 0.7) $\times 10^{11}$ cm^{-2}],[4,24–26] most likely due to reduced carrier backfilling, such designs are not conducive to high cw powers, since the maximum current density[27] J_{max} scales with doping level,[27] and the series resistance is high.

The high T_0 (260 to 278 K) and T_1 (285 K) values for the deep-well QCLs not only indicate a strong suppression of carrier leakage, but also provide indirect proof that leakage to the indirect valleys (X and/or L) is not a problem in the 4.5 to 5.0-μm range when heavily strained (≈1%) $In_{0.68}Ga_{0.32}As$ QWs are used. This confirms a recent report[28] that the X and L minima lie farther above the Γ valley than was previously

expected. Furthermore, high T_0 and T_1 are beneficial for cw operation. For example, the cw power, P_{cw}, is

$$P_{cw} = A\eta_{d,cw}(J - J_{th,cw}) = A\left[\eta_d \exp\left(-\frac{\Delta T_{act}}{T_1}\right)\right]\left[J - J_{th}\exp\left(\frac{\Delta T_{act}}{T_0}\right)\right], \quad (12)$$

where A is the device area, J is the current density, and ΔT_{act} is the temperature rise in the device core with respect to the heatsink temperature T_h, given by

$$\Delta T_{act} = T_{core} - T_h = R_{th}(AJV - P_{cw}) = R_{th}P_{cw}[(1/\eta_{wp}) - 1], \quad (13)$$

where R_{th} is the thermal resistance, T_{core} is the lattice temperature in the device core, V is the bias voltage, and $\eta_{wp} = P_{cw}/AJV$ is the cw wallplug efficiency. Equations (12) and (13) demonstrate why employing devices of high T_0 and T_1 values, such as DW-type QCLs, will be crucial for maximizing both the output power and the wallplug efficiency in RT cw operation. For example, we have estimated[29] that RT cw wallplug efficiencies in excess of 20% from a single facet become possible at 4.6 to 4.8 μm.

5 Estimates for Temperature Dependence of Threshold Current and Differential Quantum Efficiency

We use Eqs. (1) to (3) and (11) to estimate the temperature variations of J_{th} and η_d over the range 300 to 360 K. To estimate the leakage current at threshold, we calculate the electron sheet densities in states 5 and 6 using the following relations:

$$n_5 = n_{4,th}\frac{\tau_{5,tot}}{\tau_{45}} + n_6\frac{\tau_{5,tot}}{\tau_{65}}, \quad (14)$$

$$n_6 = n_5\frac{\tau_{6,tot}}{\tau_{56}}, \quad (15)$$

where $\tau_{5,tot}$ and $\tau_{6,tot}$ are the net lifetimes corresponding to electron scattering from state 5 to states 1 to 4 and 6, and from state 6 to states 1 to 5 and to states in the upper Γ miniband, respectively. The lifetime τ_{ij} corresponding to thermal excitation of electrons from a lower-energy state i to a higher-energy state j, which is predominantly due to LO-phonon absorption scattering for large energy separations, is approximated from the following expression:

$$\frac{1}{\tau_{ij}} \approx \frac{1}{\tau_{ji}}\exp\left(-\frac{E_{ji} + \hbar\omega_{LO}[(T_{ei}/T) - 1]}{kT_{ei}}\right), \quad (16)$$

where E_{ji} is the energy difference between states j and i, $\hbar\omega_{LO}$ is the LO phonon energy ($E_{ji} > \hbar\omega_{LO}$), and T_{ei} is the electronic temperature for state i, which under very low-duty-cycle operation (i.e., negligible Joule heating) is obtained from $T_{ei} - T_h = \alpha_{E\text{-}L} \cdot J$, where $\alpha_{E\text{-}L}$ is the electron-lattice coupling constant.[30] The structures used in the calculations are of the conventional [Fig. 3(a)] and deep-well [Fig. 3(b)] types, and we consider 3-mm-long, 30-period devices with uncoated facets. Since the lifetimes due to inelastic and elastic scattering tend to be similar in the λ = 4.5- to 5.0-μm range,[31] we halved the lifetimes obtained from a $k \cdot p$ code, considering only inelastic scattering, and, since the elastic-scattering lifetimes are basically temperature-independent,[4,31] we assumed that the lifetimes vary half as fast with temperature as when only inelastic scattering (that is, LO-phonon-assisted scattering) is considered. Furthermore, the presence of elastic scattering (due to interface roughness) causes the electroluminescence linewidth, $2\gamma_{43}$, to vary much more slowly than when only LO-phonon scattering is considered.[32] For example, over the 300- to 360-K temperature range, the calculated characteristic temperature coefficient for the parameter $2\gamma_{43}$ is $\approx$410 K if only LO-phonon scattering is considered,[20] in contrast with the observed value of $\approx$700 K.[32] These slower variations in τ_4 and $2\gamma_{43}$ are taken into account when calculating the temperature dependence of $J_{0,th}$. For calculating T_{ei} values we use an $\alpha_{E\text{-}L}$ value of 35 K cm^2/kA as measured[14] for the electronic temperature of the injector ground state, T_{eg}, of 4.8-μm-emitting, strain-compensated QCLs. Since state g is strongly coupled to the upper laser level, we assume that at threshold $T_{e4} \approx T_{eg}$. We also employ $T_{e5} \approx T_{e6} \approx T_{e4}$, although these assumptions may be less reliable.

Table 1 Measured and calculated parameters for conventional[3] and deep-well[13] QCLs of the DPR design (λ = 4.6 to 4.8 μm). Here J_{leak}/J_{th} is the relative electron leakage, where J_{th} is the threshold current density.

	Measured T_0 (K)	J_{leak}/J_{th}		Calculated T_0 (K)
	300 to 360 K	300 K	360 K	300 to 360 K
Conventional QCL	143	0.147	0.226	167
Deep-well QCL	253	0.088	0.128	234

Table 1 shows calculated values for the ratio J_{leak}/J_{th} at heatsink temperatures of 300 and 360 K, and for T_0, in conventional QCLs[3] and DW QCLs[13] of DPR design, with 4.6- to 4.8-μm wavelength, 30 periods, 3-mm-long cavity, and uncoated facets. For conventional QCLs of such parameters the J_{th} value at 300 K is taken to be 1.85 kA/cm^2. The value was derived from experimental data[3,5] and by using our estimates of the quantity $J_{0,th} + J_{bf,th}$ for those structures with the preceding assumptions on T_{e5} and T_{e6}, which provide a differential internal efficiency η_i of 70%. For DW QCLs the J_{th} value at 300 K for uncoated, 3-mm-long chips is 1.83 kA/cm^2.[13] Starting with the expression for $J_{0,th} + J_{bf,th}$ (i.e., $n_{4,th}/\tau_4$), we add to it the expression for $J_{leak,th}$ [Eqs. (3), (14), and (15)] and then factor out $n_{4,th}$ to find its value for a given J_{th}. Subsequently, $J_{leak,th}$ was calculated at 300 K. Then, the ratio of the value of $J_{0,th} + J_{bf,th}$ at 360 K to its value at 300 K was used as a scaling factor for $n_{4,th}$ when calculating $J_{leak,th}$ at 360 K.

The primary electron leakage path is found to be relaxation from state 5 to the lower AR states (i.e., states 3, 2, and 1) of electrons thermally excited from the upper laser level (state 4) to state 5. A secondary leakage path, which is significant only for conventional QCLs, is thermal excitation from state 6 to the upper-Γ-miniband states, and subsequently to the continuum, of electrons (thermally) excited to state 6 from state 5.

The relative carrier leakage ($J_{leak,th}/J_{th}$) is significantly smaller for DW than for conventional devices, primarily because E_{54} is 60 meV in the former and 46 meV in the latter. The higher E_{54} value, which is a consequence of the much taller barriers, affects $J_{leak,\,th}$ mostly through the scattering time τ_{45}. For example, the calculated values for τ_{45} at 360 K are 0.84 and 0.32 ps for DW-type and conventional devices, respectively. The difference is due to the E_{54} dependence in the thermal-activation term of Eq. (16), and also the larger τ_{54} value (0.21 versus 0.12 ps), which is related to the magnitude of E_{54} compared to the phonon energy (i.e., how nonresonant is the phonon-assisted scattering).

Leakage from state 6 to the continuum is basically nonexistent in DW-type devices because of the large energy difference between state 6 and the bottom of the upper Γ miniband, $E_{um,6}$ (i.e., 150 meV), as seen from Fig. 3(b), which in turn gives $\tau_{6,um}$ values of the order of 500 ps at 300 K and 200 ps at 360 K. In sharp contrast, $E_{um,6}$ in conventional devices is ≈70 meV [Fig. 3(a)], which, coupled with the significant wave-function overlap between state 6 and the lower states of the upper miniband, gives much smaller $\tau_{6,um}$ values: 2.4 ps at 300 K, and 1.3 ps at 360 K. Notwithstanding, leakage through the upper miniband at 360 K is estimated to account for only about 10% of the total $J_{leak,th}$, because of the relatively high value of E_{65} (80 meV). The electron leakage to the continuum may actually be greater if the electronic temperatures of states 5 and 6 are higher than that in the upper laser level and/or if the phonons' temperature is higher than that of the lattice temperature (i.e., hot phonons are present).

The calculated T_0 values for conventional and DW devices (167 and 234 K) agree well with the experimental values (143 and 253 K,[13] respectively). For conventional devices better agreement would be obtained if the electronic temperatures of states 5 and 6 were taken to be higher than that of state 4 and/or if α_w were taken to increase with temperature. Conversely, for DW devices a lower (injector) ground-state electronic temperature T_{eg} and thus better agreement is expected, since lower $\alpha_{E\text{-}L}$ values are associated with higher conduction-band offsets.[14] With increasing temperature, lower T_{eg} values would decrease both $J_{bf,th}$ and $J_{leak,th}$, which together with increases in α_w would provide more accurate T_0 values for DW devices.

T_1 values are estimated from the η_d expression (11) by assuming that only η_p varies with temperature, and using calculated T_0 values for the quantity $J_{0,th} + J_{bf,th}$ combined with the derived T_0 values for the total J_{th}. For conventional devices the T_1 value thus obtained is 585 K, much higher than expected, although no direct comparisons with experiment could be made, since in the literature we could not find pulsed *L-I* curves beyond $T = 298$ K for 4.6- to 4.8-μm QCLs of the DPR design. (A T_1 value of ≈153 K can be derived from pulsed *L-I* curves[33] covering $T = 280$ to 298 K.) While pulsed *L-I* curves for 4.6 to 4.8-μm-emitting devices of other designs yield $T_1 \approx 143$ K over the 273 to 323-K range for the bound-to-continuum design[23] and 140 K over the 293- to 333-K range for the NRE design,[2] direct comparisons are not possible. Nonetheless a discrepancy exists, which may be due to the same reasons as for the higher calculated T_0 values; that is, higher electronic temperatures for upper AR states and α_w increasing with temperature, with the latter having a stronger influence, since α_w variations affect the η_d value much more than the J_{th} value. For DW devices the estimated T_1 value is 1260 K, much higher than the experimental result of 285 K,[13] which may in part be due to a lower T_{eg} value and in a larger part due to α_w increasing with temperature.

Finally, by using a modified equation for the maximum wallplug efficiency $\eta_{wp,max}$,[29] which takes into account the leakage-induced droop in the pulsed light-versus-*J* curve,[17] and the differential pumping-efficiency term η_p, and considers that the maximum in pulsed wallplug efficiency occurs at a current density $J_{wp,max}$ smaller than J_{max} [viz., $J_{wp,max} \approx 2.5 \times J_{th}(300\ \text{K})$],[6,33]—most likely due to leakage currents high above threshold via injection into upper AR states,[34]—we calculated, for an optimized DW-QCL structure with $N_p = 40$ and optimal α_m value 2.2 cm^{-1} (just as in Ref. 17), a pulsed $\eta_{wp,max}$ value of ≈23.5% for front-facet-emitted (i.e., usable) power at 300 K. This is ≈1.7 times higher than the best reported front-facet values for conventional QCLs.[17] Then, by assuming similar thermal and electrical resistances to those in Ref. 17 and using Eqs. (12) and (13), the temperature rise in the device core with respect to the heatsink temperature, ΔT_{act}, is estimated to be ≈21 K for DW QCL devices at the point where the wallplug efficiency reaches its maximum in cw operation at 300 K. In contrast, for conventional QCLs,[6] which have significantly lower T_0 and T_1 values than DW QCLs, by using Eq. (13) the value of ΔT_{act} at $\eta_{wp,max}$ is found to be ≈30 K. Then, for DW QCLs, by using the estimated ΔT_{act} and the experimentally measured T_0 and T_1 values, we estimate a maximum front-facet, RT cw wallplug efficiency value of ≈22%.

6 Conclusions

The use of deep quantum wells in the active regions of mid-infrared QCLs has resulted in the strong suppression of electron leakage. This is evidenced by significantly lower temperature sensitivities for both the threshold current and the slope efficiency than in conventional QCLs. Basically, both the threshold current and the slope efficiency of DW QCLs vary with temperature about 2.3 times slower than those parameters for conventional, high-performance QCLs. This dramatic suppression of carrier leakage indicates that we are approaching temperature dependences determined mainly by inelastic and elastic scattering and backfilling. The virtual doubling of T_0 and T_1 above room temperature should lead to significantly improved cw performance as well as better long-term reliability at watt-range cw powers. Furthermore, the achieved carrier leakage suppression makes DW-QCL designs ideally suited for incorporation into intersubband quantum-box laser structures.

The conventional equations for threshold current and external differential quantum efficiency have been modified to reflect both electron leakage and backfilling when the electrons in the injectors are hot. The calculated T_0 values for both conventional and DW QCLs are in good agreement with experiment, providing evidence that our thermal-excitation model involving hot electrons in both the injector and the active region is correct.

Acknowledgments

This work was supported in part by the National Science Foundation under grant ECCS-0925104. The authors are grateful to Jerome Faist for valuable technical discussions.

References

1. J. Faist, F. Capasso, C. Sirtori, D. Sivco, and A. Cho, "Intersubband transitions in quantum wells: physics and device applications II," Chap. 1 in *Semiconductors and Semimetals*, H. Liu and F. Capasso, Eds. 66 pp. 1–83, Academic, New York (2000).
2. A. Lyakh, C. Pflugl, L. Diehl, Q. J. Wang, F. Capasso, X. J. Wang, J. Y. Fan, T. Tanbuk-Ek, R. Maulini, A. Tsekoun, R. Go, and C. K. N. Patel, "1.6 W high wallplug efficiency, continuous-wave, room temperature quantum cascade laser emitting at 4.6 μm," *Appl. Phys. Lett.* **92**, 111110 (2008).
3. Y. Bai, S. R. Darvish, S. Slivken, W. Zhang, A. Evans, J. Nguyen, and M. Razeghi, "Room temperature continuous wave operation of quantum cascade lasers with watt-level optical power," *Appl. Phys. Lett.* **92**, 101105 (2008).
4. C. Pflügl, L. Diehl, A. Lyakh, Q. J. Wang, R. Maulini, A. Tsekoun, C. Kumar N. Patel, X. Wang, and F. Capasso, "Activation energy study of electron transport in high performance short wavelengths quantum cascade lasers," *Opt. Express* **18**, 746–753 (2010).
5. Y. Bai, S. Slivken, S. R. Darvish, and M. Razeghi, "Room temperature continuous wave operation of quantum cascade lasers with 12.5% wall plug efficiency," *Appl. Phys. Lett.* **93**, 021103 (2008).
6. A. Lyakh, R. Maulini, A. Tsekoun, R. Go, C. Pflügl, L. Diehl, Q. J. Wang, Federico Capasso, and C. Kumar N. Patel, "3 W continuous-wave room temperature single-facet emission from quantum cascade lasers based on nonresonant extraction design approach," *Appl. Phys. Lett.* **95**, 141113 (2009).
7. J. Faist, "Wallplug efficiency of quantum cascade lasers: critical parameters and fundamental limits," *Appl. Phys. Lett.* **90**, 253512 (2007).
8. P. Q. Liu, A. J. Hoffman, M. D. Escarra, K. J. Franz, J. B. Khurgin, Y. Dikmelik, X. Wang, J.-Y. Fan, and C. F. Gmachl, "Highly power-efficient quantum cascade lasers," *Nature Photon.* **4**, 95–98 (2010).
9. Y. Bai, S. Slivken, S. Kuboya, S. R. Darvish, and M. Razeghi, "Quantum cascade lasers that emit more light than heat," *Nature Photon.* **4**, 99–102 (2010).
10. J. Faist, "Quantum cascade lasers circuits," *Int. Quantum Cascade Lasers School & Workshop* (2010). http://www.physique.univ-paris-diderot.fr/iqclsw/.
11. D. P. Xu, M. D'Souza, J. C. Shin, L. J. Mawst, and D. Botez, "InGaAs/GaAsP/AlGaAs, deep-well, quantum-cascade light-emitting structures grown by metalorganic chemical vapor deposition," *J. Crystal Growth* **310**, 2370–2376 (2008).
12. J. C. Shin, M. D'Souza, Z. Liu. J. Kirch, L. J. Mawst, D. Botez, I. Vurgaftman, and J. R. Meyer, "Highly temperature insensitive, deep-well 4.8 μm emitting quantum cascade semiconductor lasers," *Appl. Phys. Lett.* **94**, 201103 (2009).
13. J. C. Shin, L. J. Mawst, D. Botez, I. Vurgaftman, and J. R. Meyer, "Ultra-low temperature sensitive, deep-well quantum-cascade lasers ($\lambda = 4.8\ \mu$m) via uptapering conduction band edge of injector regions," *Electron. Lett.* **45**, 741 (2009).
14. M. S. Vitiello, T. Gresch, A. Lops, V. Spagnolo, G. Scamarcio, N. Hoyler, M. Giovannini, and J. Faist, "Influence of InAs, AlAs δ layers on the optical, electronic, and thermal characteristics of strain-compensated GaInAs/AlInAs quantum-cascade lasers," *Appl. Phys. Lett.* **91**, 161111 (2007).
15. P. M. Smowton and P. Blood, "The differential efficiency of quantum-well lasers," *IEEE J. Sel. Top. Quantum Electron.* **3**, 491–498 (1997).
16. J. S. Yu, S. Slivken, A. J. Evans, and M. Razeghi, "High-performance continuous-wave operation of $\lambda \sim 4.6\ \mu$m quantum-cascade lasers above room temperature," *IEEE J. Quantum Electron.* **44**, 747–754 (2008).
17. R. Maulini, A. Lyakh, A. Tsekoun, R. Go, C. Pflügl, L. Diehl, F. Capasso, C. Kumar N. Patel, "High power thermoelectrically cooled and uncooled quantum cascade lasers with optimized reflectivity facet coatings," *Appl. Phys. Lett.* **95**, 151112 (2009).
18. L. Diehl, D. Bour, S. Corzine, J. Zhu, G. Hofler, B. G. Lee, C. Y. Wang, M. Troccoli, and F. Capasso, "Pulsed- and continuous-mode operation at high temperature of strained quantum-cascade lasers grown by metalorganic vapor phase epitaxy," *Appl. Phys. Lett.* **88**, 041102 (2006).
19. J. C. Shin, M. D'Souza, D. Xu, J. Kirch, L. J. Mawst, D. Botez, I. Vurgaftman, and J. R. Meyer, "Characteristics of deep-well 4.8 μm-emitting quantum-cascade lasers grown by MOCVD," *Proc. SPIE* **7230**, 723013 (2009).
20. C. -F. Hsu, J. -S. O, P. Zory, and D. Botez, "Intersubband quantum-box semiconductor lasers," *IEEE J. Sel. Top. Quantum Electron.* **6**, 491–503 (2000).
21. D. Botez, G. Tsvid, M. D'Souza, J. C. Shin, Z. Liu, J. H. Park, J. Kirch, L. J. Mawst, M. Rathi, T. F. Kuech, I. Vurgaftman, J. Meyer, J. Plant, G. Turner, and P. Zory, "Intersubband quantum-box lasers: progress and potential as uncooled mid-infrared sources," in *Future Trends in Microelectronics: From Nanophotonics to Sensors to Energy*, S. Luryi, J. Xu, and A. Zaslavksy, Eds., pp. 49–64, Wiley-IEEE Press, (2010).
22. J. C. Shin, M. D'Souza, J. Kirch, J. H. Park, L. J. Mawst, and D. Botez, "Characteristics of mid-IR-emitting deep-well quantum cascade lasers grown by MOCVD," *J. Crystal Growth* **312**, 1379–1382 (2010).
23. T. Gresch, J. Faist, and M. Giovannini, "Gain measurements in strain-compensated quantum cascade laser," *Appl. Phys. Lett.* **94**, 161114 (2009).
24. L. Diehl, D. Bour, S. Corzine, J. Zhu, G. Höfler, M. Loncar, M. Troccoli, and F. Capasso, "High-temperature continuous wave operation of strain-balanced quantum cascade lasers grown by metal organic vapor-phase epitaxy," *Appl. Phys. Lett.* **89**, 081101 (2006).
25. A. Evans, J. S. Yu, S. Slivken, and M. Razeghi, "Continuous-wave operation of $\lambda \sim 4.8\ \mu$m quantum-cascade lasers at room temperature," *Appl. Phys. Lett.* **85**, 2166–2168 (2004).
26. A. Evans, J. Nguyen, S. Slivken, J. S. Yu, S. R. Darvish, and M. Razeghi, "Quantum-cascade lasers operating in continuous-wave mode above 90°C at $\lambda \sim 5.25\ \mu$m," *Appl. Phys. Lett.* **88**, 051105 (2006).
27. C. Sirtori, F. Capasso, J. Faist, A. Hutchinson, D. Sivco, and A. Cho, "Resonant tunneling in quantum cascade lasers," *IEEE J. Quantum Electron.* **34**, 1722 (1998).
28. G. Molis, A. Krotkus, and V. Vaičaitis, "Intervalley separation in the conduction band of InGaAs measured by terahertz excitation spectroscopy," *Appl. Phys. Lett.* **94**, 091104 (2009).
29. D. Botez, S. Kumar, J. C. Shin, L. J. Mawst, I. Vurgaftman, and J. R. Meyer, "Temperature dependence of the key electro-optical characteristics for midinfrared emitting quantum cascade lasers," *Appl. Phys. Lett.* **97**, 071101 (2010).
30. V. Spagnolo, G. Scamarcio, H. Page, and C. Sirtori, "Simultaneous measurement of the electronic and lattice temperatures in $GaAs/Al_{0.45}Ga_{0.55}As$ quantum-cascade lasers: influence on the optical performance," *Appl. Phys. Lett.* **84**, 3690 (2004).
31. J. Faist, private communication.
32. A. Wittmann, Y. Bonetti, J. Faist, E. Gini, and M. Giovannini, "Intersubband linewidths in quantum cascade laser designs," *Appl. Phys. Lett.* **93**, 141103 (2008).
33. M. Razeghi, "High-power high-wallplug efficiency mid-infrared quantum cascade lasers based on the InP/GaInAs/AlInAs material system," *Proc. SPIE* **7230**, 723011 (2009).
34. Y. Dikmelik, J. B. Khurgin, P. Q. Liu, M. D. Escarra, A. J. Hoffman, K. J. Franz, and C. F. Gmachl, "Limitations to the power output and efficiency of mid-infrared quantum cascade lasers imposed by transport," in *Tech. Dig. 2010 IEEE/OSA CLEO Conf.*, Paper JTuD88 (2010).

Dan Botez received the BS degree with highest honors and the MS and PhD degrees in electrical engineering from the University of California, Berkeley, in 1971, 1972, and 1976, respectively. In 1977 he joined RCA Laboratories, Princeton, NJ, where his research concentrated on new types of high-power, single-mode AlGaAs/GaAs lasers, which became commercial products. In 1986 he joined TRW, Inc., Redondo Beach, CA, where he was senior staff scientist and technical fellow. At TRW he was coinventor of the concept of resonant leaky-wave coupling in phase-locked arrays of antiguides (1988), which led to the first active photonic crystal (APC) laser structure for single spatial-mode operation from wide-aperture (>100-μm) devices. As a result, in 1990 he led the team that broke the 1-W coherent-power barrier for diode lasers. In 1993 he became the Philip Dunham Reed Professor of Electrical Engineering and director of the Reed Center for Photonics at the University of Wisconsin–Madison. At UW-Madison, his work on Al-free lasers has led to record-high cw power and wallplug efficiency from diode lasers. Recent work has focused on two-dimensional APC-type lasers and quantum cascade lasers. He is a fellow of the IEEE and of the Optical Society of America (OSA). In 1979 he received an RCA Outstanding Achievement Award for codevelopment of high-density optical recording using diode lasers. As part of the the IEEE centennial (1984) events, he was chosen the Outstanding Young Engineer of the IEEE Photonics Society. In 1995 he was awarded the doctor honoris causa degree by the Polytechnical University of Bucharest, Romania, and in 2010 he received the OSA Nick Holonyak Jr. Award. He has authored or coauthored more than 270 refereed publications; holds 48 patents with 2 pending; and has given 90 invited presentations.

Jae Cheol Shin received his BS and MS degrees in physics from Kyung Hee University, Yongin, Korea, in 2001 and 2003, respectively. Then he received his PhD degree in electrical engineering from the University of Wisconsin–Madison in 2010. At University of Wisconsin–Madison his research focused on highly temperature-insensitive, deep-well quantum cascade lasers, as well as III-V semiconductor growth using metal-organic chemical vapor deposition (MOCVD). Since graduation, he has been working in the Electrical and Computer Engineering Department at the University of Illinois at Urbana-Champaign as a postdoctoral fellow pursuing research in InGaAs nanowire growth using MOCVD for various electronic- and photonic-device applications.

Sushil Kumar received a BE degree from the Delhi College of Engineering, Delhi (1998), a MS degree from the University of Michigan, Ann Arbor (2001), and a PhD degree from Massachusetts Institute of Technology, Cambridge (2007), all in the field of electrical engineering. His PhD thesis work involved various aspects of the development of terahertz quantum-cascade lasers (QCLs). Following three years of postdoctoral work at the Research Laboratory of Electronics, Massachusetts Institute of Technology, he has been an assistant professor in the Department of Electrical and Computer Engineering at the Lehigh University in Bethlehem, PA, since the fall of 2010. His present research interests are in the area of terahertz photonics and technology, intersubband semiconductor devices, and silicon photonics.

Luke J. Mawst received the BS degree in engineering physics and the MS and PhD degrees in electrical engineering from the University of Illinois at Urbana-Champaign in 1982, 1984, and 1987, respectively. His dissertation research involved the development of index-guided semiconductor lasers and laser arrays grown by MOCVD. He joined TRW, Inc., Redondo Beach, CA, in 1987, where he was a senior scientist in the TRW Research Center, engaged in design and development of semiconductor lasers using MOCVD crystal growth. He is coinventor of the resonant optical waveguide (ROW) antiguided array and has contributed to its development as a practical source of high coherent power, for which he received the TRW Group Level Chairman's Award. He developed a novel single-mode edge-emitting laser structure, the ARROW laser, as a source for coupling high powers into single-mode optical fibers. He is currently a professor in the Electrical and Computer Engineering Department at the University of Wisconsin–Madison, where he is involved in the development of novel III-V compound semiconductor device structures, including vertical-cavity surface emitters (VCSELs), active photonic lattice structures, dilute-nitride lasers, solar cells, and high-power Al-free diode lasers. He is a founder of Alfalight Inc, a Madison-based manufacturer of high-power diode lasers. Prof. Mawst has authored or coauthored more than 200 technical papers and holds 20 patents. He is a senior member of the IEEE.

Igor Vurgaftman received the BS degree summa cum laude in computer engineering from Boston University in 1991, and the MS and PhD degrees in electrical engineering from the University of Michigan in 1993 and 1995, respectively. His dissertation research dealt with the electronic and optical properties of quantum structures with reduced dimensionality and modification of spontaneous emission in microcavity lasers. Since 1995 Dr. Vurgaftman has been with the Optical Sciences Division of the Naval Research Laboratory (NRL), Washington, DC. At NRL, he has investigated mid-infrared lasers based on interband and intersubband transitions, methods of maintaining optical coherence in large-area semiconductor lasers, type II superlattice photodetectors, coherent sources of surface plasmons, and spintronic optical and electronic devices, among other topics. His 2001 review of the band parameters for III-V semiconductors [I. Vurgaftman and J. R. Meyer, *J. Appl. Phys.* **89**, 5815 (2001)] has been cited more than 1500 times. He is the author of more than 200 refereed articles in technical journals, numerous contributed and invited talks at professional conferences, and 12 patents.

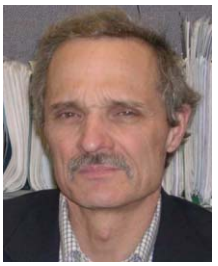

Jerry R. Meyer completed his PhD in physics at Brown University in 1977. Since then he has carried out basic and applied research at the Naval Research Laboratory in Washington, DC, where he is now head of the Quantum Optoelectronics Section. He was recently appointed to the position of Senior Scientist for Quantum Electronics (ST). His investigations have focused on semiconductor optoelectronic materials and devices, such as the development of new classes of semiconductor lasers and detectors for the infrared. He is a fellow of the Optical Society of America, the American Physical Society, the Institute of Electrical and Electronics Engineers, and the Institute of Physics. He has coauthored more than 320 refereed journal articles, which have been cited more than 6800 times (H-Index 35); 13 book chapters; 22 patents awarded and pending; and more than 110 invited conference presentations.